A&A 415, 1065–1072 (2004)
DOI: 10.1051/0004-6361:20031668

Astronomy & Astrophysics

The NH_3 / N_2H^+ abundance ratio in dense cores⋆

S. Hotzel[1], J. Harju[1], and C. M. Walmsley[2]

[1] Observatory, PO Box 14, 00014 University of Helsinki, Finland
[2] Osservatorio Astrofisico di Arcetri, Largo E. Fermi 5, 50125 Firenze, Italy

Received 19 June 2003 / Accepted 18 December 2003

Abstract. We have observed the dense cores Barnard 217 (B217) and LDN 1262 (L1262) in the $(J, K) = (1, 1)$ and $(2, 2)$ inversion lines of ammonia and in the $J = 1$–0 rotational line of diazenylium. The two cores are morphologically similar, in the sense that both contain a Class-I young stellar object (YSO) 1–2′ away from the core centre. The NH_3 and N_2H^+ column densities show the same pattern in both cores: the average NH_3/N_2H^+ abundance ratios are 140–190 in the starless main bodies of the cores, while they drop to about 60–90 in the regions around the YSOs. Comparison with the dust continuum emission of B217 suggests that this pattern is due to an enhanced fractional ammonia abundance in the quiescent part of the core, where we find $N(NH_3)/N(H_2) = 5 \times 10^{-8}$. On the outskirts of the core the fractional ammonia abundance is about 3×10^{-8}, in accordance with our previous results. We discuss these findings in the light of recent chemical models including molecular depletion.

Key words. ISM: individual objects: Barnard 217 – ISM: individual objects: LDN 1262 – ISM: abundances – ISM: molecules

1. Introduction

The nitrogenous compounds ammonia (NH_3) and diazenylium (N_2H^+) have again in recent years engaged the attention of researchers of cold condensations in interstellar molecular clouds. The reason is that these molecules do not seem to be very susceptible to freezing out onto dust grains, and therefore they can be used as tracers of the physical conditions of pre-stellar and protostellar clumps. This behaviour was predicted by Charnley (1997) and by Bergin & Langer (1997) with the aid of chemical models, and has been observationally established in several depletion studies towards dark cores (e.g. Willacy et al. 1998; Caselli et al. 1999; Tafalla et al. 2002; Bergin et al. 2002). In these regions NH_3 and N_2H^+ correlate with the dust continuum emission better than other molecules observed. A large scale correlation between N_2H^+ and NH_3 towards TMC-1 has been reported by Hirahara et al. (1995).

It is not clear, however, whether the distributions of the two species are similar in the interiors of dense cores. In the study of Bergin et al. (2002), N_2H^+ shows evidence for slight depletion towards the centre of Barnard 68. Tafalla et al. (2002) infer from their observations towards several dark cloud cores that while N_2H^+ has a constant fractional abundance, the abundance of NH_3 increases towards the core centres. Also Caselli et al. (2002) find that NH_3 and N_2H^+ do not always peak at the same place.

The spectral lines of NH_3 and N_2H^+ show hyperfine structure due to the electric quadrupole moment of the N nucleus. This facilitates the estimation of their optical thicknesses and excitation temperatures, and the derivation of the physical conditions in their origin. The spectroscopic and chemical properties of N_2H^+ and NH_3 make them important tracers of dense cores. In view of the fact that some recent studies have suggested differences in their ability to withstand depletion, it seems important to study their relative distributions in detail.

In this paper we present the results of NH_3 and N_2H^+ mapping of two dense cores, Barnard 217 (B217) and LDN 1262 (L1262)[1], initially detected in ammonia by Myers & Benson (1983) and Benson & Myers (1989). Recently these cores were observed in N_2H^+ (Benson et al. 1998; Caselli et al. 2002), but the angular resolution of these data was not sufficient to derive the abundance distributions within the cores. We have re-observed the cores in N_2H^+ to complement our earlier ammonia maps of 40″ resolution. Our ammonia map of B217 has been published previously (Hotzel et al. 2001).

The two cores have similar morphologies: they both contain a Class-I source (Lada & Wilking 1984; Lada 1987; Chen et al.1995; Yun & Clemens 1995) 1–2′ off from a dense, possibly pre-stellar nucleus. Both cores are also at similar distances from the sun, B217 at 140 pc (Elias 1978), L1262 at 180 pc (Kun 1998), so that our resolution refers to similar physical scales. We find that in both cores the N_2H^+ to NH_3 column density ratios are different in the direction of the YSOs and the core centres. On the basis of the dust continuum map of B217

Send offprint requests to: S. Hotzel,
e-mail: hotzel@astro.helsinki.fi

⋆ Based on observations with the 100-m telescope of the MPIfR (Max-Planck-Institut für Radioastronomie) at Effelsberg, and with the 20-m telescope of the Onsala Space Observatory at Onsala.

[1] LDN 1262 actually covers a larger region. Another identifier for the part of LDN 1262 studied here is [CB88] 244 (Clemens & Barvainis 1988).

(Motte & André 2001) we suggest that the difference is caused by an increase in the ammonia abundance in the quiescent core centre. We discuss possible reasons for this increase at the end of this paper.

2. Observations and data analysis

The ammonia observations were carried out in 1988 with the Effelsberg 100-m telescope (40″ beam at 23.7 GHz). Observational details can be found in Hotzel et al. (2001).

The diazenylium observations were made in 2003 with the Onsala 20-m telescope (41″ beam at 93.2 GHz) using the SIS 100-GHz receiver. The system temperature including the atmosphere was 370–1010 K during alternating weather conditions. The spectrometer was a 1600 channel autocorrelator with a band-width of 40 MHz, corresponding to a channel-width of 0.08 km s^{-1}. The pointing and focus were checked at 4–6 h intervals towards circumstellar SiO($v = 1, J = 2$–1) maser line sources, and the pointing accuracy was found to be better than 6″. The observations were performed in the frequency switching mode, and calibration was done by the chopper wheel method. We used the elevation dependent beam efficiencies (0.44–0.56) provided by the telescope team to convert the observed antenna temperatures T_A^* to main beam temperatures T_{MB}. In L1262 the map spacing was 20″; the total integration time per position was usually between 6 and 12 min but it was between 24 and 56 min for the central positions. In B217 the map spacing was 28″, and the integration time was 6 min in all but 3 central positions, where the integration time reached up to 114 min. The noise levels lie typically around 0.4 K (rms(T_{MB})) for the shorter integration times and around 0.1 K for the very long integration times. Sample spectra are shown in Fig. 1.

At each position, we have modeled hyperfine spectra to the data, assuming equal excitation temperatures and beam filling factors for the individual hyperfine components (see also Fig. 1). The filter frequency response function was taken into account when deriving the best model spectra in χ^2-fits to the data. The four unknown variables are the excitation temperature T_{ex}, the total opacity τ_0, the line-of-sight velocity V_0 and the line-width ΔV, except for the $NH_3(J, K) = (2, 2)$ line, where we have assumed $T_{ex}^{22} = T_{ex}^{11}$ and $\Delta V_{22} = \Delta V_{11}$. Here and in the following, the indices "10", "11" and "22" refer to the $N_2H^+(J = 1$–$0)$, $NH_3(J, K) = (1, 1)$ and $NH_3(J, K) = (2, 2)$ transitions, respectively.

To derive T_{ex}^{11} and T_{ex}^{10} one needs to know the beam filling factors of the sources, which are assumed to be unity. Depending on the extent of the emission and the existence of unresolved small scale structure in the sources, the beam filling factors may be over- or underestimated. The subsequent uncertainties in the column densities do not affect the results of this study significantly. In particular the NH_3/N_2H^+ abundance ratio is not affected at all, as a difference between the beam filling factors of the two molecules (observed with the same beam) is very unlikely.

The χ^2-fits failed to produce reliable results in about 2/3 of all observed positions, due to a low signal-to-noise ratio (*SNR*). Therefore, we used the line areas, *A*, for deriving ammonia and diazenylium column densities at all positions in the following way: by means of the positions with derived T_{ex} and ΔV, we have fixed typical values of these parameters (for ammonia, also the rotational temperature, T_{12}, describing the relative populations of the metastable ($J = K$) rotational levels) in either core and for either species. With the approximation of these variables being constant within the sources, there are unique relations between *A* and τ_0. After deriving τ_0 at all positions, we have calculated the column densities following for NH_3 the concept first presented by Ho et al. (1979), and using for N_2H^+ the approximation of a linear, rigid rotator in LTE. The final equations are:

$$N(NH_3) = \frac{3\sqrt{\pi}\,h\varepsilon_0}{2\pi^2\sqrt{\ln 2}\,\mu_{NH_3}^2}\,\frac{e^{\frac{h\nu}{kT_{ex}}}+1}{e^{\frac{h\nu}{kT_{ex}}}-1} \times\left(\frac{1}{3}e^{\frac{23.4\,K}{T_{12}}}+1+\frac{5}{3}e^{-\frac{41.5\,K}{T_{12}}}+\frac{14}{3}e^{-\frac{101.1\,K}{T_{12}}}\right)\Delta V\,\tau_0\,, \quad (1)$$

where ν, T_{ex}, ΔV and τ_0 are the frequency, excitation temperature, line-width and total opacity of the $NH_3(J, K) = (1, 1)$ inversion transition respectively, and

$$N(N_2H^+) = \frac{3\sqrt{\pi}\,h\varepsilon_0}{2\pi^2\sqrt{\ln 2}\,\mu_{N_2H^+}^2}\,\frac{e^{\frac{h\nu}{kT_{ex}}}}{e^{\frac{h\nu}{kT_{ex}}}-1}\left(\frac{kT_{ex}}{h\nu}+\frac{1}{6}\right)\Delta V\,\tau_0\,, \quad (2)$$

where ν, T_{ex}, ΔV and τ_0 are the frequency, excitation temperature, line-width and total opacity of the N_2H^+ $J = 1$–0 rotational transition respectively. $\mu_{NH_3} = 1.476$ debye (Poynter & Kakar 1975) is the electric dipole moment of NH_3, and $\mu_{N_2H^+} = 3.4$ debye (Green et al. 1974) the one of N_2H^+. The constants *h*, *k* and ε_0 have their usual meanings.

3. Results

For the N_2H^+ observations, we have selected two positions in each core, where we have integrated for a particularly long time in order to reach a high *SNR*: at the peak position of our NH_3 maps and at those positions observed in NH_3 which are closest to the YSOs. The corresponding results of the χ^2-fits are summarised in Table 1, where the columns are: (1) name of the source and position identification: "Core" stands for the centre of the starless main body of the core. "YSO" stands for the selected position close to the YSO. (2) Line of sight velocity in the N_2H^+ transition with respect to the local standard of rest (LSR).[2] (3–4) Line-widths in the observed transitions ($\Delta V^{22} = \Delta V^{11}$). The instrumental broadening is implicitly taken into account. (5–7) Total opacities. (8–9) Excitation temperatures ($T_{ex}^{22} = T_{ex}^{11}$). The physical parameters, derived directly from the values in Table 1, are given in Table 2, where the columns are: (1) source name as in Table 1. (2) N_2H^+ column density. (3) NH_3 column density. (4) Kinetic temperature, derived from the NH_3 data. (4) H_2 number density, derived from the NH_3 data.

Our column density maps are presented in Figs. 2 (L1262) and 3 (B217). As average parameters (based on the χ^2-fits) we

[2] The NH_3 velocities are omitted, because the absolute velocities of these spectra are uncertain by ∼0.1 km s^{-1} due to an earlier data conversion software problem.

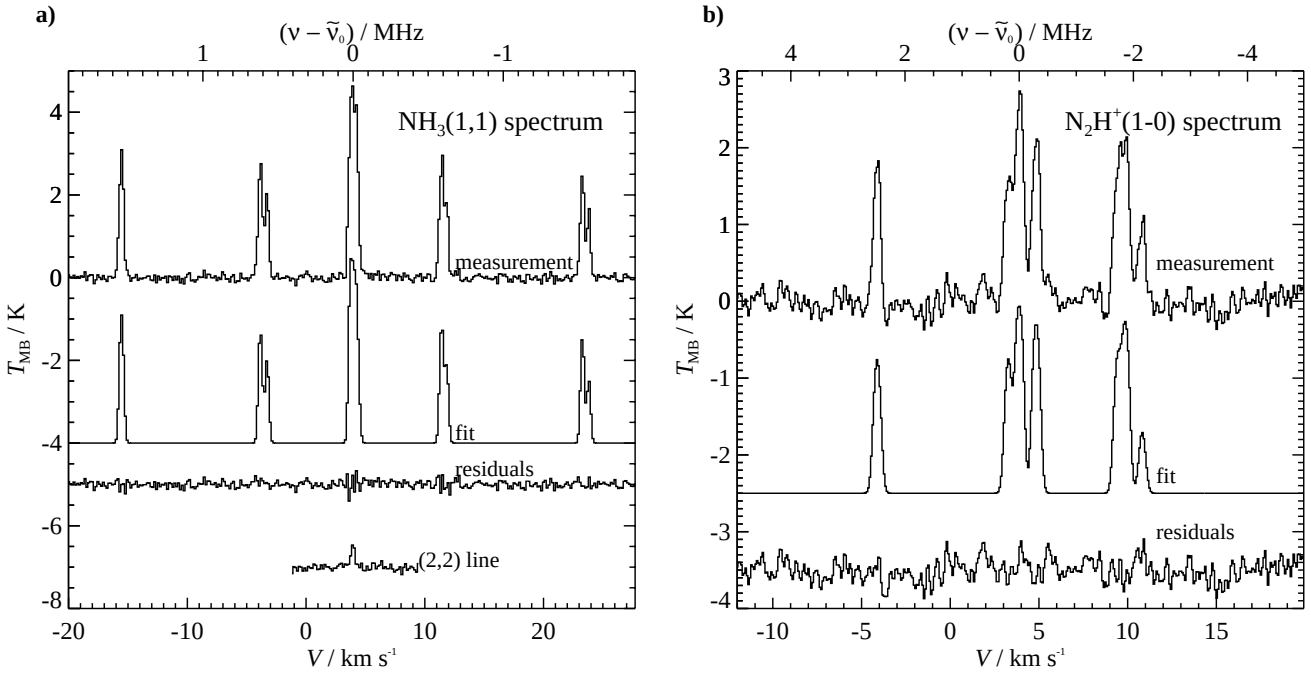

Fig. 1. a) $NH_3(J,K) = (1,1)$ and $(2,2)$ spectra and **b)** $N_2H^+(J = 1–0)$ spectrum at our reference position of L1262, $\alpha(2000) = 23^h25^m29\overset{s}{.}7$, $\delta = +74°18'15''$.

Table 1. Results of the χ^2-fits with 1-σ formal errors. The error is to be read as the fit-value ± the number in parentheses in the same decimal power as the last given decimal digit of the fit-value. τ_0 is the *total opacity* of the transition, i.e. the sum of the central opacities of the individual hyperfine components of the transition in question.

Source-Position	V_0^{10} (km s^{-1})	ΔV^{10} (km s^{-1})	ΔV^{11} (km s^{-1})	τ_0^{10}	τ_0^{11}	τ_0^{22}	$T_{ex}^{10\,a}$ (K)	$T_{ex}^{11\,a}$ (K)
(1)	(2)	(3)	(4)	(5)	(6)	(7)	(8)	(9)
L1262-Core[b]	3.886(5)	0.42(1)	0.315(4)	9.7(10)	12.0(4)	0.20(2)	5.7(6)	7.4(10)
L1262-YSO[c]	4.085(8)	0.46(2)	0.497(27)	12.8(17)	5.1(8)	0.27(7)	5.0(5)	6.5(9)
B217-Core[d]	7.009(4)	0.33(1)	0.321(4)	4.4(9)	7.3(2)	0.17(2)	7.0(10)	10.2(15)
B217-YSO[e]	7.514(6)	0.41(2)	0.310(28)	2.0(3)	2.5(12)	0.13(10)	7.4(11)	7.6(19)

[a] A 20% uncertainty in T_A^* is included in the error calculation, the uncertainty in the beam filling factor is not.
[b] RA $23^h25^m29\overset{s}{.}7$, Dec $+74°18'15''$ (2000.0). [d] RA $04^h27^m46\overset{s}{.}5$, Dec $+26°17'52''$ (2000.0).
[c] RA $23^h25^m44\overset{s}{.}5$, Dec $+74°17'35''$ (2000.0). [e] RA $04^h27^m56\overset{s}{.}9$, Dec $+26°19'31''$ (2000.0).

Table 2. Physical parameters calculated from the results of the χ^2-fits. Numbers in parentheses are 1-σ errors as in Table 1.

Source-Position	$N(N_2H^+)$ (10^{13} cm^{-2})	$N(NH_3)$ (10^{15} cm^{-2})	T_{kin} (K)	$n(H_2)$ (10^4 cm^{-3})
(1)	(2)	(3)	(4)	(5)
L1262-Core	1.6(3)	2.4(4)	8.6(1)	>2.7[a]
L1262-YSO	1.9(4)	0.9(3)	11.4(9)	1.6(7)
B217-Core	0.8(3)	1.8(3)	9.3(1)	>15.9[a]
B217-YSO	0.5(2)	–[b]	–[b]	–[b]

[a] The method to estimate the molecular Hydrogen density (Eq. (2) of Ho & Townes 1983) fails if the density gets high enough to thermalise the (1, 1) transition. Lower limits are then calculated by using $T_{ex}^{11} - \sigma(T_{ex}^{11})$ and $T_{kin} + \sigma(T_{kin})$.
[b] *SNR* of the NH_3 data too low.

used in L1262: $T_{ex}^{11} = 7$ K, $T_{12} = 9$ K, $\Delta V^{11} = 0.35$ km s^{-1}, $T_{ex}^{10} = 5.5$ K, $\Delta V^{10} = 0.4$ km s^{-1}, and in B217: $T_{ex}^{11} = 9.5$ K, $T_{12} = 9.5$ K, $\Delta V^{11} = 0.3$ km s^{-1}, $T_{ex}^{10} = 7$ K, $\Delta V^{10} = 0.35$ km s^{-1}.

3.1. L1262

In Fig. 2a, white contours of N_2H^+ column density are overlaid on an image of NH_3 column density (pronouncing black contours show the same data as the image). The shape of the globule in the lower level contours is similar in NH_3 and N_2H^+. In the higher level contours though, there is a distinction between NH_3 and N_2H^+. While NH_3 peaks in one sharp maximum 2′ northwest of the YSO, N_2H^+ has got two maxima. One is close to the NH_3 maximum, and a second one is less than 1′ away from the YSO. The NH_3 map has a shoulder towards the

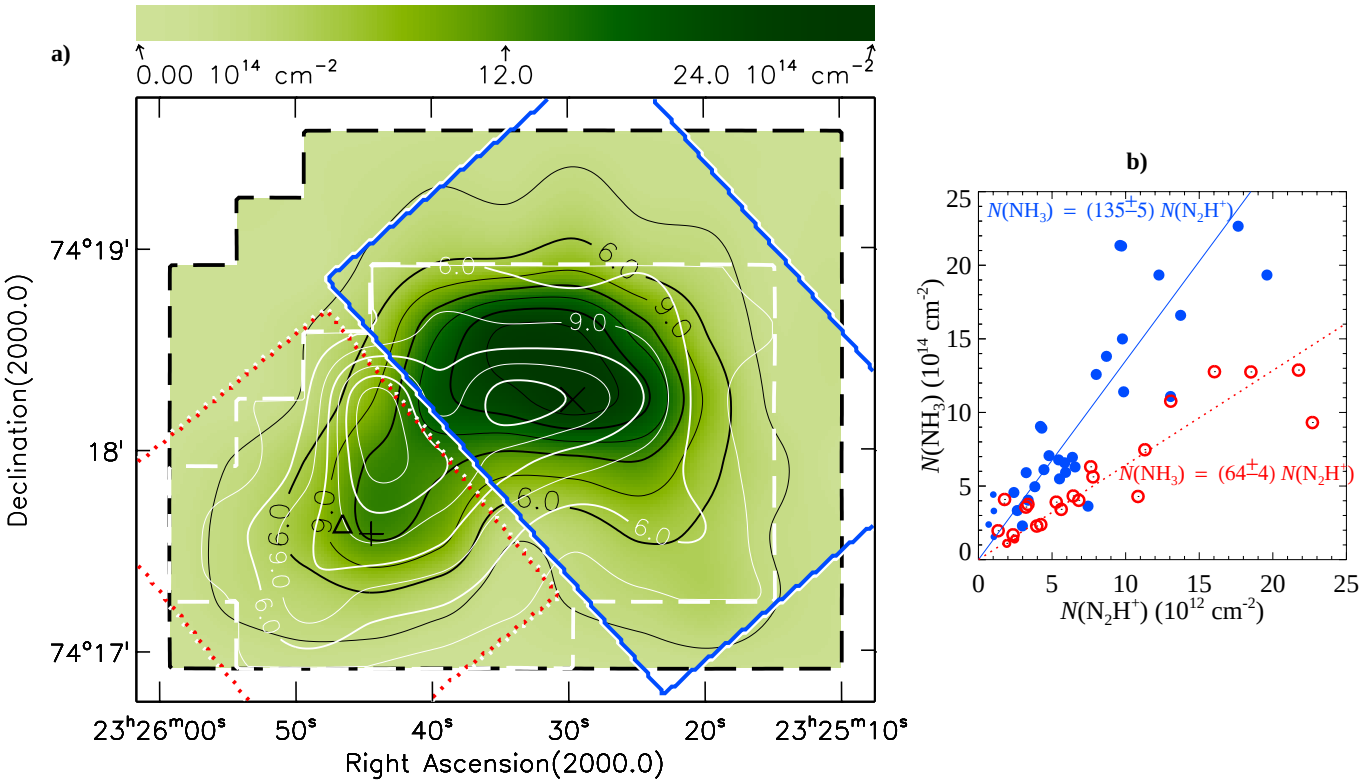

Fig. 2. a) N_2H^+ (white contours) and NH_3 (image and black contours) column density maps of L1262. The range of $N(NH_3)$ is indicated by the colour bar at the top of the figure, and contours run from 3.0 to 21.0×10^{14} cm^{-2} in steps of 3.0×10^{14} cm^{-2}. Contours of $N(N_2H^+)$ are drawn from 3.0 to 21.0×10^{12} cm^{-2} in steps of 3.0×10^{12} cm^{-2}. The triangle marks the position of the YSO (IRAS 23238+7401). The cross and the plus sign mark the positions with long integration times in N_2H^+(J = 1–0) (see Fig. 1). The dotted (red) frame and the solid (blue) frame identify the regions L1262-YSO and L1262-Core respectively. The two regions are arbitrarily selected on the basis of the data presented in this figure. It is suggested that L1262-YSO is a star-forming part of L1262, while L1262-Core is quiescent. **b)** $N(NH_3)$ vs. $N(N_2H^+)$ correlation plot for L1262. Filled (blue) circles are data from L1262-Core, open (red) circles are data from L1262-YSO. Data points with $SNR < 3$ in either transition are marked with small symbols. The relations between the two molecules are approximated by linear functions, treating the two regions separately. The solid lines are fitted to the 3-sigma data points by least-squares minimisation of both, x-offsets and y-offsets. The slopes of the lines are given in the figure.

position of the second N_2H^+ peak, but no secondary maximum can be seen. To quantify this finding, we have defined two regions within L1262, in which we compare the two observed molecules. The first one, L1262-YSO, is approximately centred on the YSO and includes the corresponding peak in N_2H^+ and the shoulder of the NH_3 distribution. The second, larger one, L1262-Core, includes the main body of the NH_3 core. The two regions represent the star-forming and the quiescent part of L1262 and are outlined in Fig. 2a by a dotted (red) frame and a solid (blue) frame respectively.

Ammonia and diazenylium column densities are compared in Fig. 2b. Fitting straight lines to the data points, we find the average NH_3/N_2H^+ relative abundances in the two regions: $[NH_3]/[N_2H^+] \approx 140$ in L1262-Core and $[NH_3]/[N_2H^+] \approx 60$ in L1262-YSO.

3.2. B217

The results of our observations of B217 are shown in Fig. 3a, where white contours of $N(N_2H^+)$ and black contours of $N(NH_3)$ are overlaid on an image of the dust continuum at 240 GHz (1.2 mm) (Motte & André 2001).

All 3 tracers presented in Fig. 3a show the same main features of B217[3]: the main body of the dense core has a size of $\sim3' \times 2'$, is elongated in northeast–southwest direction and is centred on $\alpha(2000) = 4^h27^m47^s, \delta = +26°18'$. Separated by a narrow valley of low emission, there is a secondary core with a size of $\sim1'$, centred on $\alpha = 4^h28^m56^s$, $\delta = +26°19'30''$. This smaller core is located on the axis of elongation of the main core and harbours the Class-I source IRAS 04248+2612. Proceeding as in Sect. 3.1, we define the two regions containing the structures just described by a solid (blue) frame and a dotted (red) frame in Fig. 3a, and name them B217-Core and B217-YSO respectively.

We compare the ammonia and diazenylium column densities in Fig. 3b. As for L1262, the $N(NH_3)$ vs. $N(N_2H^+)$ data points are approximated by straight lines. $[NH_3]/[N_2H^+] \approx 190$ in B217-Core and $[NH_3]/[N_2H^+] \approx 90$ in B217-YSO.

[3] The whole structure shown in Fig. 3a is named B217 throughout this paper for simplicity. It is only part of the larger dark core structure as seen in the optical, and is to be identified with the earlier designations B217-1 (Lee & Myers 1999) and B217SW (Hotzel et al. 2001).

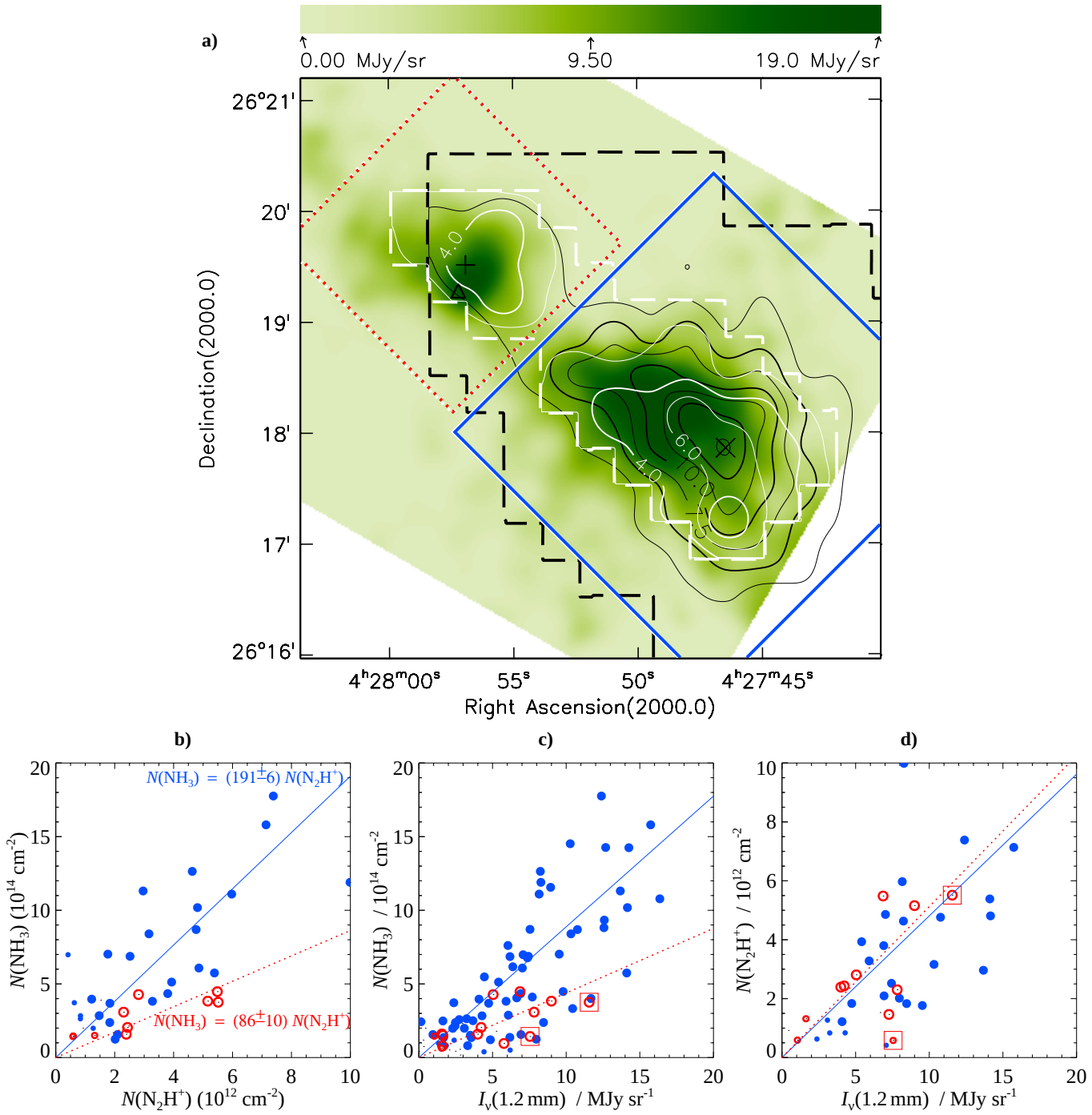

Fig. 3. a) N_2H^+ (white) and NH_3 (black) column density contours overlaid on the 240 GHz (1.2 mm) dust continuum map (Motte & André 2001) of B217. The N_2H^+ and NH_3 beams are about 40″, while the 1.2 mm map has 20″ resolution. The colour bar at the top of the figure indicates the range of I_ν(1.2 mm). Contours of $N(NH_3)$ are drawn from 2.5 to 17.5×10^{14} cm^{-2} in steps of 2.5×10^{14} cm^{-2}, and contours of $N(N_2H^+)$ run from 2.0 to 8.0×10^{12} cm^{-2} in steps of 2.0×10^{12} cm^{-2}. The triangle marks the position of the YSO (IRAS 04248+2612). The cross and the plus sign mark the positions with long integration times in N_2H^+(J = 1–0). The dotted (red) frame and the solid (blue) frame identify the regions B217-YSO and B217-Core respectively. The two regions are arbitrarily selected on the basis of the data presented in this figure. It is suggested that B217-YSO is a star-forming part of B217, while B217-Core is quiescent. **b–d)** Column density correlation plots for B217. Filled (blue) circles are data from B217-Core, open (red) circles are data from B217-YSO. **b)** $N(NH_3)$ vs. $N(N_2H^+)$. Symbols have the same meaning as in Fig. 2b. The relations between the two molecules are approximated by linear functions, treating the two regions separately. The correlation factors are given in the figure. **c)** $N(NH_3)$ vs. I_ν(1.2 mm) and **d)** $N(N_2H^+)$ vs. I_ν(1.2 mm). Data points with SNR < 3 in the molecular line are marked with small symbols. The straight lines are fitted to only those data points which satisfy this criterion. Large boxes mark data points closer than 24″ to the YSO.

The NH_3/N_2H^+ ratios in B217 behave in a similar fashion as those in L1262: the NH_3/N_2H^+ abundance ratio in B217-Core is significantly higher than the one in B217-YSO, most likely by a factor 2–3. The same result was found for the difference between the quiescent and the star-forming part of L1262. The absolute values of the NH_3/N_2H^+ ratios are about 30% lower in L1262 than in B217, which is a small difference compared to the abundance variations within the sources.

In B217, we can also compare the molecular abundances with the dust column density. We defer the discussion of the shortcomings in converting the 1.2 mm continuum to dust and subsequently H_2 column densities to Sect. 4 and compare at first our two molecular species with the 1.2 mm *intensities*. After smoothing the continuum data to 40″ resolution, we get from Figs. 3c–d the following results: in B217-Core, the ammonia abundance is $N(NH_3)/I_\nu(1.2\,\mathrm{mm}) = 90\times10^{14}\ \mathrm{cm^{-2}\ MJy^{-1}\ sr}$, while in B217-YSO it drops to about half of this value. The diazenylium abundance (relative to $I_\nu(1.2\,\mathrm{mm})$) in B217-Core is approximately 200 times lower than the ammonia abundance, and in B217-YSO it is roughly 100 times lower than the ammonia abundance. This last result was to be expected from the earlier direct NH_3/N_2H^+ comparison. Important to note at this point, is that it is the N_2H^+ molecule, which has a roughly constant abundance relative to the continuum emission over the whole globule, while NH_3 shows a significant difference in its abundances relative to $I_\nu(1.2\,\mathrm{mm})$ between B217-Core and B217-YSO.

4. Discussion

4.1. Fractional molecular abundances

The fractional ammonia abundance $\chi(NH_3) \equiv N(NH_3)/N(H_2)$ in B217 was derived by Hotzel et al. (2001). Carrying out a near-infrared (NIR) reddening analysis using the Two Micron All Sky Survey (Cutri 1997), they derived $\chi(NH_3) = (2.9\pm1.2)\times10^{-8}$. The field stars used in that analysis are all situated outside the $2.5\times10^{14}\ \mathrm{cm^{-2}}$ contour (see Fig. 3a), so the dense parts of the core were not sampled.

Here we use the continuum map to estimate the hydrogen column densities. As the dust emission is optically thin at mm wavelengths, it is proportional to the hydrogen column density as far as the dust temperature, T_dust, and the dust absorption cross section per hydrogen nucleus, $\sigma^\mathrm{H}_{1.2\,\mathrm{mm}}$, remain constant throughout the cloud:

$$\begin{aligned} N(H_2) &= \frac{I_\nu(1.2\,\mathrm{mm})}{2\sigma^\mathrm{H}_{1.2\,\mathrm{mm}} B_\nu(T_\mathrm{dust})} \\ &= 1.8\times10^{21}\ \mathrm{cm^{-2}}\times\left(\frac{I_\nu(1.2\,\mathrm{mm})}{\mathrm{MJy\,sr^{-1}}}\right) \\ &\quad\times\left(\frac{B_\nu(T_\mathrm{dust})}{B_\nu(12\,\mathrm{K})}\right)^{-1}\times\left(\frac{\sigma^\mathrm{H}_{1.2\,\mathrm{mm}}}{2.0\times10^{-26}\,\mathrm{cm^2}}\right)^{-1}. \end{aligned} \quad (3)$$

In the first line of the equation we applied the approximation that all hydrogen is in molecular form. The dust temperature of B217 was taken from Hotzel et al. (2001, $T_\mathrm{dust} = 12.0^{+1.9}_{-1.0}$ K for B217-Core). The value for $\sigma^\mathrm{H}_{1.2\,\mathrm{mm}}$ was suggested by Ossenkopf & Henning (1994, $\kappa_{1.3\,\mathrm{mm}} = 0.8\,\mathrm{cm^2/g}$) for cores of density $n_\mathrm{H} \approx 10^5\ \mathrm{cm^{-3}}$ (we assumed a gas-to-dust mass ratio of 100 and 70% of the gas, in mass, being hydrogen).

Unfortunately both quantities, T_dust and $\sigma^\mathrm{H}_{1.2\,\mathrm{mm}}$ may vary within the cloud. In a starless dense core, the dust temperature is expected to decrease towards the centre (Leung 1975; Evans et al. 2001; Zucconi et al. 2001), while in an internally heated envelope of a protostar, it will decrease outwards (e.g. Terebey et al. 1993). The former case holds for B217-Core, while the latter one may hold to some degree for B217-YSO. As however the luminosity of the YSO is low, its influence on the dust temperature should vanish 13″ from the source (Motte & André 2001). Away from the immediate surrounding of the YSO, the dust temperature distributions and in fact the average dust temperatures may thus be the same in B217-YSO and in B217-Core. In the correlation study with NH_3 and N_2H^+ we used a 40″ resolution version of the dust map, so any effect of a modestly increased dust temperature would be smeared out over an area of $\approx\sqrt{(13'')^2+(20'')^2} = 24''$ in radius. The two observed positions within this area are marked by large squares in Figs. 3c–d, but they do not show up suspiciously in the scatter plots, and omitting them would not alter the results significantly.

At densities $n_\mathrm{H} > 10^5\ \mathrm{cm^{-3}}$ the dust opacity is expected to increase with increasing density due to a more efficient coagulation process. However, Ossenkopf & Henning (1994) calculated that for the most realistic ice-coated dust grains, this increase should be well below a factor 2. A direct global influence of the protostar in B217-Core on the dust opacity is also unlikely because of its low luminosity. It is thus possible that T_dust and $\sigma^\mathrm{H}_{1.2\,\mathrm{mm}}$ vary somewhat within B217, but there are no reasons to assume significant differences between B217-Core and B217-YSO.

Combining Eq. (3) with the results from Figs. 3c–d, we find

$$\chi(NH_3) = (4.9\pm0.5)\times10^{-8}\left(\frac{B_\nu(T_\mathrm{dust})}{B_\nu(12\,\mathrm{K})}\right)\left(\frac{\sigma^\mathrm{H}_{1.2\,\mathrm{mm}}}{2.0\times10^{-26}\,\mathrm{cm^2}}\right) \quad (4)$$

and

$$\chi(N_2H^+) = (2.6\pm0.5)\times10^{-10}\left(\frac{B_\nu(T_\mathrm{dust})}{B_\nu(12\,\mathrm{K})}\right)\left(\frac{\sigma^\mathrm{H}_{1.2\,\mathrm{mm}}}{2.0\times10^{-26}\,\mathrm{cm^2}}\right) \quad (5)$$

in B217-Core. For B217-YSO the numerical values are $(2.4\pm0.4)\times10^{-8}$ in Eq. (4) and $(2.8\pm0.3)\times10^{-10}$ in Eq. (5).

4.2. Radial profiles

In Figs. 2b and 3b–d differences between the Core- and the YSO-regions are apparent regarding the average NH_3/N_2H^+ abundance ratio and regarding the average NH_3/dust ratio, while the average N_2H^+/dust ratio remains the same. Looking for differences *within* the cores, Fig. 4 shows the radial profiles of the mentioned column density ratios.

In Figs. 4a and 4b, $N(NH_3)/N(N_2H^+)$ is plotted as function of the projected distance from the centres of L1262 and B217 respectively. In B217-Core the two molecules peak at different positions, so the profile is not monotonic and has a

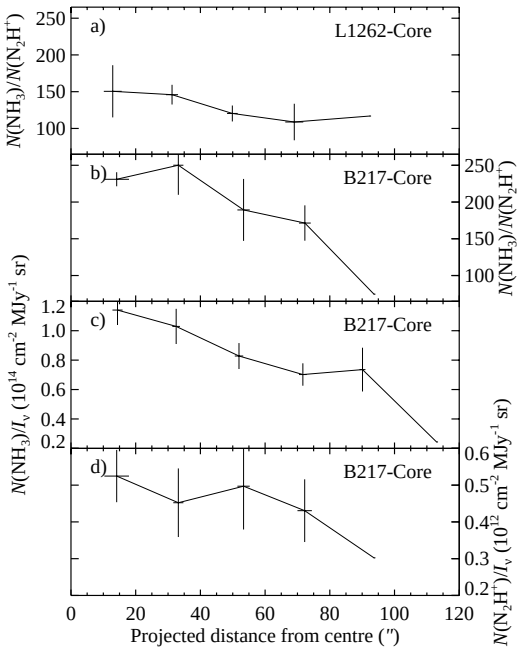

Fig. 4. Radial profiles of the column density ratios. **a)** $N(NH_3)/N(N_2H^+)$ in L1262-Core as function of projected distance from the central position $\alpha(2000) = 23^h25^m31\overset{s}{.}0$, $\delta = +74°18'20''$. The data are averaged in annuli of 20″ width. The averages are non-weighted, but only 3-sigma detections have been used. The assigned error bars are statistical error bars (1-sigma uncertainty of the mean). Averages are also calculated in the *x*-axis, in order to plot the points at the best-corresponding radius values. Where no error bars are assigned, there is only one data point in the bin. The purpose of the line connecting the 5 points is to guide the eye. **b)** $N(NH_3)/N(N_2H^+)$ vs. projected radius in B217-Core. The selected central position is $\alpha(2000) = 4^h27^m47\overset{s}{.}0$, $\delta = +26°17'59''$. The symbols have the same meaning as before. **c)** $N(NH_3)/I_\nu(1.2\,\mathrm{mm})$ and **d)** $N(N_2H^+)/I_\nu(1.2\,\mathrm{mm})$ in B217-Core. The central position and the meaning of the symbols are the same as in b).

larger scatter than in L1262-Core. Also the absolute values of $N(NH_3)/N(N_2H^+)$ are larger in B217 than in L1262. But in both cores the profiles show a decrease with distance from the centre: between the centres and 80″ projected distance by ≈40%. This decrease is small compared with the earlier established difference between the Cores and the YSO-regions.

In Figs. 4c–d, the profiles involving the mm continuum emission are shown. For constant $T_{\rm dust}$ and $\sigma^{\rm H}_{1.2\,\rm mm}$, c) and d) are proportional to the ammonia and diazenylium fractional abundance profiles respectively. Both profiles decrease with distance from the centre, but up to a distance of 80″, only for NH_3 this decrease is statistically robust. The scatter in $\chi(N_2H^+)$ is large, because the sharp N_2H^+ peak is far off the dust peak, or in other words the approximation of circular symmetry is not a very good one. In the framework of this approximation, $\chi(N_2H^+)$ may as well be constant in B217-Core.

It should be mentioned that the outer contours of $N(NH_3)$ and $N(N_2H^+)$ are centred on almost the same position (which is close to the NH_3-peak and was chosen as central position in Fig. 4), and that only the N_2H^+ peak position is off centre. Between the molecular contours and the dust contours however, there is a more general shift of about 20″. As the pointing accuracy in all observations involved is around 5″, this shift is likely to be real. Possible explanations include 1) temperature or dust opacity gradients and 2) molecular abundance gradients. In any case, the shift underlines that B217-Core is not spherical and that its radial profiles must be treated with caution. It is however noteworthy that the same trends for $N(NH_3)/N(N_2H^+)$, $N(NH_3)/I_\nu(1.2\,\mathrm{mm})$ and $N(N_2H^+)/I_\nu(1.2\,\mathrm{mm})$, that have been detected earlier between the starless cores and the YSO-regions, do also exist between the centres and the outer regions of the cores themselves.

4.3. Chemistry

The main production pathways of N_2H^+ and NH_3 in the gas phase are presented in Fig. 5 (cf. e.g. Le Bourlot 1991; Nejad & Wagenblast 1999). Diazenylium is closely related to molecular nitrogen through electrons and the H_3^+ ions, and it has been used to infer the N_2 abundance in molecular clouds (Womack et al. 1992a,b). In fact most nitrogen is supposed to be in the form of N_2, which is produced in relatively slow neutral-neutral reactions. Nitrogen atoms are replenished through the dissociative reaction $N_2 + He^+ \rightarrow N^+ + He + N$. The N^+ ions lead to ammonia (see Fig. 5). Also the reactions of N with the H_2^+ (or possibly H_3^+) ions can produce precursors of ammonia.

The observed persistence of gaseous N_2H^+ and NH_3 in dense cores of molecular clouds is thought to be based on the relatively low binding energies of N and N_2 on dust grains, which allow them to evaporate more easily than species containing O or C. Recent observations and modelling results suggest furthermore that conditions where most of the heavy molecules are depleted favour the formation of N_2H^+ and NH_3: according to Aikawa et al. (2003), N_2 can be formed on grain surfaces and then desorbed into the gas phase, while at the same time the diminished abundances of CO and other heavy molecules decrease the destruction of N_2H^+ itself and of H_3^+ and He^+, which are necessary for the formation of N_2H^+ and NH_3. As a consequence, the abundances of diazenylium and ammonia increase with increasing density, with the tendency being more marked for N_2H^+. In contrast to these model results, Tafalla et al. (2002) found a flat N_2H^+ abundance distribution in the starless core L1544, while NH_3 seemed to peak towards the core centre (see also Fig. 8 of Aikawa et al. 2003).

The higher NH_3 / N_2H^+ column density ratio towards the cores of B217 and L1262, and the fact that N_2H^+ correlates on average with the dust emission in B217 harmonise with the results of Tafalla et al. (2002) and thereby give further support to their suggestion that ammonia is somehow enhanced in quiescent cores with high degrees of molecular depletion.

While the possible processes behind the rise of NH_3 and N_2H^+ abundances were discussed by Aikawa et al. (2003), the process behind the increase of ammonia relative to diazenylium remains so far unspecified. One explanation – if the surface reactions suggested by Aikawa et al. (2003) are not efficient – is that OH is under-abundant causing a reduction in N_2 production. This in turn reduces the N_2H^+ abundance while pathways to ammonia from atomic nitrogen are still viable.

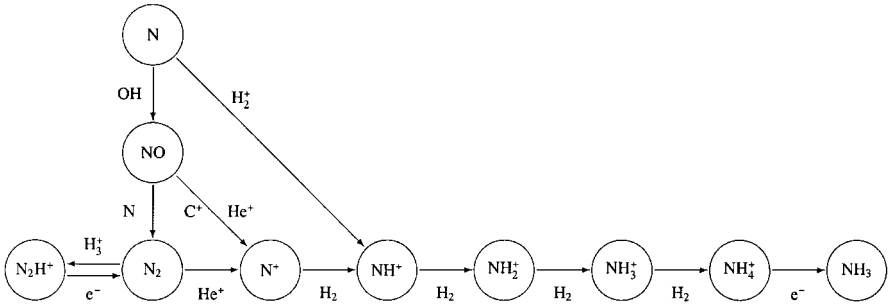

Fig. 5. The main reaction routes to N_2H^+ and NH_3 in the gas phase.

Another finding of Aikawa et al. (2003) is that in a collapsing core, accretion onto dust grains will finally affect NH_3 when the central density reaches $\sim 10^6$ cm^{-3}, whereas N_2H^+ remains unaffected almost all the way during collapse from 3×10^4 to 3×10^7 cm^{-3} central density. According to their Fig. 3, the interesting consequence for the *column* densities is, that a golden period for ammonia, when $N(NH_3)$ is at its maximum, is followed by a golden period for diazenylium, when after 2×10^5 years of collapse the central density has reached 3×10^7 cm^{-3} and $N(N_2H^+)$ is at its maximum. Comparing our findings for the NH_3/N_2H^+ abundance ratios in B217 and L1262 to these modelling results, it is tempting to interpret the differences between the starless and the star forming regions as manifestations of their different evolutionary stages. If this is true, the abundance ratio of these two molecules could become a tool to probe the evolutionary stage of dense and prestellar cores. However, as neither $N(H_2)$ nor $N(N_2H^+)$ is higher in B217-YSO than in B217-Core, there is no overall agreement with the results of Aikawa et al. (2003). Hence the two regions cannot represent evolutionary stages of cores starting from the same initial conditions (they must have had at least different masses initially), and the pertinence of the model quoted for the interpretation of our results is uncertain.

5. Summary

We have mapped the dense cores L1262 and B217 in NH_3 and N_2H^+. Comparing the molecular abundances, we have found the same results in both objects: the NH_3/N_2H^+ abundance ratios are at least twice as large in the dense and starless parts of the cores than in the regions closer to the YSOs.

Comparison with the dust continuum shows that the fractional ammonia abundance rises above 5×10^{-8} in the starless areas, while the fractional diazenylium abundance remains at a level around 2.5×10^{-10}. An enhanced ammonia abundance in environments where CO and other heavy molecules are frozen out onto dust grains could be explained by a reduced destruction rate of the molecular ions H_3^+ and He^+, which are necessary for the formation of N_2H^+ and NH_3. A reduced OH abundance could be responsible for a lower N_2 production rate, which would limit the subsidiary effect on the N_2H^+ production while the NH_3 production could continue.

Acknowledgements. We are grateful to Dr. Frédérique Motte for providing us with the mm-continuum map of B217. This project was supported by the Academy of Finland, grant No. 73727 and 74854.

References

Aikawa, Y., Ohashi, N., & Herbst, E. 2003, ApJ, 593, 906
Benson, P. J., & Myers, P. C. 1989, ApJS, 71, 89
Benson, P. J., Caselli, P., & Myers, P. C. 1998, ApJ, 506, 743
Bergin, E. A., & Langer, W. D. 1997, ApJ, 486, 316
Bergin, E. A., Alves, J., Huard, T., & Lada, C. J. 2002, ApJ, 570, L101
Caselli, P., Walmsley, C. M., Tafalla, M., Dore, L., & Myers, P. C. 1999, ApJ, 523, L165
Caselli, P., Benson, P. J., Myers, P. C., & Tafalla, M. 2002, ApJ, 572, 238
Charnley, S. B. 1997, MNRAS, 291, 455
Chen, H., Myers, P. C., Ladd, E. F., & Wood, D. O. S. 1995, ApJ, 445, 377
Clemens, D. P., & Barvainis, R. 1988, ApJS, 68, 257
Cutri, R. M. 1997, in The Impact of Large Scale Near-IR Sky Surveys, ed. F. Garzon, N. Epchtein, & A. Omont, ASSL, 210, 187
Elias, J. H. 1978, ApJ, 224, 857
Evans, N. J., Rawlings, J. M. C., Shirley, Y. L., & Mundy, L. G. 2001, ApJ, 557, 193
Green, S., Montgomery, J. A., & Thaddeus, P. 1974, ApJ, 193, L89
Hirahara, Y., Masuda, A., Kawaguchi, K., et al. 1995, PASJ, 47, 845
Ho, P. T. P., & Townes, C. H. 1983, ARA&A, 21, 239
Ho, P. T. P., Barrett, A. H., Myers, P. C., et al. 1979, ApJ, 234, 912
Hotzel, S., Harju, J., Lemke, D., Mattila, K., & Walmsley, C. M. 2001, A&A, 372, 302
Kun, M. 1998, ApJS, 115, 59
Lada, C. J. 1987, in Star Forming Regions, ed. M. Peimpert, & J. Jugaku (D. Reidel Publishing Company), Proc. IAU Symp, 115, 1
Lada, C. J., & Wilking, B. A. 1984, ApJ, 287, 610
Le Bourlot, J. 1991, A&A, 242, 235
Lee, C. W., & Myers, P. C. 1999, ApJS, 123, 233
Leung, C. M. 1975, ApJ, 199, 340
Motte, F., & André, P. 2001, A&A, 365, 440
Myers, P. C., & Benson, P. J. 1983, ApJ, 266, 309
Nejad, L. A. M., & Wagenblast, R. 1999, A&A, 350, 204
Ossenkopf, V., & Henning, T. 1994, A&A, 291, 943
Poynter, R. L., & Kakar, R. K. 1975, ApJS, 29, 87
Tafalla, M., Myers, P. C., Caselli, P., Walmsley, C. M., & Comito, C. 2002, ApJ, 569, 815
Terebey, S., Chandler, C. J., & Andre, P. 1993, ApJ, 414, 759
Willacy, K., Langer, W. D., & Velusamy, T. 1998, ApJ, 507, L171
Womack, M., Ziurys, L. M., & Wyckoff, S. 1992a, ApJ, 387, 417
Womack, M., Ziurys, L. M., & Wyckoff, S. 1992b, ApJ, 393, 188
Yun, J. L., & Clemens, D. P. 1995, AJ, 109, 742
Zucconi, A., Walmsley, C. M., & Galli, D. 2001, A&A, 376, 650